SvedbergOpen
DISSEMINATION OF KNOWLEDGE
International Journal of Artificial Intelligence and Machine Learning
Publisher's Home Page: https://www.svedbergopen.com/
Research Paper Open Access

Advances In Bone Health Analysis Using Deep Learning On Dexa Scan Images For Postmenopausal Osteoporosis

Priyanandhini V (Corresponding Author)[1] , Dr.Thilagavathy R[2]

[1]Department of Computer Applications, College of Science and Humanities,SRM Institute of Science And Technology, Kattankulathur,Tamilnadu, India pv0348@srmist.edu.in , Orcid id - 0009-0006-5609-7878
[2]Assistant Professor, Department of Computer Applications, College of Science And Humanities, SRM Institute of Science And Technology, Kattankulathur,Tamil Nadu,India thilagar1@srmist.edu.in , Orcid id - 0009-0006-1180-7194

Abstract
Postmenopausal osteoporosis (POP), a progressive bone condition that puts patients at risk for fragility fractures, is characterized by decreasing bone mineral density (BMD) and altered bone microarchitecture. The ability of the conventional diagnostic instruments, which are mostly based on BMD measurements, to assess fracture risk and examine intricate bone structure patterns is restricted. To get over these restrictions, this research suggests a novel, medically informed deep learning model for thorough osteoporosis diagnosis and fracture analysis based on dual-energy X-ray absorptiometry (DEXA) pictures. The proposed model employs a multi-task learning framework that integrates osteoporosis severity evaluation, fracture point detection, and bone segmentation into a unified model. To achieve anatomically correct bone segmentation, a bidirectional U-Net is employed, and in scenarios where insufficient labeled samples are available, a self-supervised feature pretraining strategy enhances feature representation. A temporal dependency module is employed to model the retrieved features, and a spatial attention-based convolutional neural network is employed to enhance them in order to analyze subtle spatial and structural variations in regions of low bone mass. Additionally, a cross-attention fusion module is employed to integrate numerical BMD information with image-derived features to achieve a comprehensive and medically valid fracture risk evaluation that transcends BMD measurements. The TransResNet model based on attention enhances the reliability of models and makes it possible to estimate the confidence level of diagnostic predictions. High performance is proved by the experimental assessment of the model on the DEXA datasets, with accuracy of 98.96%, sensitivity of 98.26%, and specificity of 98.43%. The effectiveness of the model in identifying osteoporotic fractures and the severity of the disease is proved by the clinical validation of the model by orthopedic experts. The findings demonstrate that the suggested framework greatly improves diagnostic accuracy and reliability, demonstrating the potential of the most recent deep learning techniques to support early intervention, individualized treatment planning, and precise computer-aided osteoporosis diagnosis.

Keywords: Postmenopausal osteoporosis Diagnosis, bidirectional U-Net, cross-attention fusion ,

1. Introduction

Osteoporosis is referred to as "porous bone" (OP). OP is a bone-related disorder that gets worse when bone quality or structure changes, which can result in fractures, or when bone mineral density (BMD) decreases. OP is a serious safety issue that needs a lot of resources to deal with the short-term and long-term effects of fractures. Elderly people are the main victims of osteoporosis; women are more susceptible than males because of hormonal changes that hasten bone loss, particularly in postmenopausal women [1. Fractures are more likely, either implicitly or as a result of external factors, especially in the hip, wrist, and spine parts. Reduced height, leaning forward, shallow breaths, and lower back pain are typical signs of OP. Everyone's risk of osteoporosis-related bone fractures rises with age, particularly postmenopausal women and women over 50. Certain ethnic groups, such as Asian and Caucasian women, are more likely to develop osteoporosis. Osteoporosis risk factors include bariatric surgery, hormone therapy, multiple myeloma, inflammatory bowel disease, and overactive thyroid, parathyroid, or adrenal glands [2]. Osteoclasts adhere to the surface of the bone and breakdown the mineral matrix, allowing calcium and other minerals to enter the blood [3]. Old or diseased bone tissue is removed during this process. Osteoblasts enter the resorbed area after resorption and secrete new bone matrix, mostly collagen, which eventually mineralizes. The structural integrity of the bone is restored by this new bone tissue. The term "bone diseases" refers to a broad category of conditions that impact the strength, structure, and functionality of bones. Weakened

bones, fractures, discomfort, and other consequences can result from these disorders. Bone illnesses can significantly lower quality of life since they affect strength, mobility, and overall health. Strong bones are maintained and the likelihood of bone problems is decreased by early diagnosis, effective treatment, and preventative measures such a balanced diet, frequent exercise, and sufficient calcium and vitamin D intake [4].

The weakening of bones, which increases their susceptibility to fractures and other problems, is the main cause of osteoporosis's extensive consequences on the body [5]. The hip, spine, and wrist are prominent fracture sites for osteoporotic bones, which are especially vulnerable to fractures even from little falls or stress. Hip fractures can cause impairment or even death in elderly people and are frequently serious enough to require surgery or long-term care. Spinal fractures frequently result in decreased mobility, balance problems, and discomfort. They can also cause height loss, kyphosis (hunched posture), and persistent back pain. Fractures can significantly limit a person's range of motion, leading to a loss of independence, particularly in the hips and spine. After a catastrophic fracture, many people may require long-term care or assistance with everyday tasks. A lower quality of life can also result from physical restrictions brought on by pain, immobility, and fractures. By accurately identifying and segmenting osteopenia/osteoporosis from X-ray/DEXA images, preprocessing, feature extraction, and segmentation/classification approaches are creatively applied to increase diagnosis accuracy. Clinicians can get information on low bone mass using several traditional procedures, but they are less accurate and require a lot of processing time. The developed automated algorithms produced high-quality, richly informative recognized and segmented regions from the input precise identification of the osteopenia/osteoporosis region of interest from the multimodal pictures provided by the proposed approaches [14–18]. The radiologists and doctors confirm and authenticate the segmentation results from the clinical X-ray and DEXA pictures. The challenges in identifying abnormalities in medical photographs are the driving force for this study. Clinicians and radiologists must hasten scanning, anomaly diagnosis, and report preparation due to the large number of patients attending imaging/scan centers. Errors can occasionally arise via manual interventions, but they can be recognized and minimized. In order to enable clinicians to start therapy as quickly as feasible, the exact demarcation of any abnormalities in the image should be supplied as a report. The efficacy of the created algorithms in identifying and analyzing the unhealthy (osteopenic/osteoporotic) bone sections is demonstrated in this work using clinical X-ray and DEXA datasets. Healthcare professionals can evaluate the efficacy of osteoporosis therapy and make appropriate modifications by routinely assessing BMD using various imaging modalities [19-20]. The objectives of the proposed models are

- To develop a deep learning model UNet, with attention-based TransResNet model, for medical image segmentation and classification of low bone mass conditions.
- To assess how well the suggested model performs in correctly dividing and categorizing bone health into groups for norm al, osteopenia, or osteoporosis.
- To analyze the effectiveness of the hybrid strategy in improving the diagnosis and visualization of low bone mass conditions.

The following are the sections: The survey of deep learning techniques applied to medical image processing is listed in Section 2. Techniques for augmentation, detection, and segmentation that aid in grade recognition in medical image analysis are described in Section 3. The results and unresolved issues are examined in Section 4. Section 5 concludes the paper.

2. Review of literature

Kim et al. developed a novel method for reconstructing bone microstructures from CT imaging data combining topology optimization and finite element analysis. Their method minimizes compliance while recreating trabecular microarchitecture in particular volumes of interest (VOIs) by utilizing Wolff's law, which highlights the self-optimizing characteristics of bone. A restriction on BMD deviation from quantitative CT (QCT) data is included to preserve patient-specific bone distribution [6]. By increasing the resolution of QCT scans from 625 μm to 62.5 μm, this technique provides a more realistic representation of bone microstructure [7].

Using artificial intelligence techniques, Jennane et al. created a classification system for individuals with osteoarthritic and osteoporotic disorders. Here, the hybrid skeleton graph technique is used to examine bone form and structure, while finite element analysis (FEA) is used for topological detection. Lastly, classification is done using AI methods like SVM, ANFIS, and GA, of which GA has a higher success rate. A novel algorithm was developed by Boughida et al. to identify and tag the different emotional expressions on people's faces [8]. Concurrently, the best features are selected and the optimal Support Vector Machine hyperparameter values are determined using gabor filters and a genetic algorithm. This outperforms other methods now in use for recognizing human face expressions in terms of recognition rates. A face detection

technique was developed by Hammouche et al. using the Gabor Filter and Sparse Auto Encoder. There are seven open in total.

To categorize patients with osteoporotic illnesses with and without vertebral bone fractures, Valentinitsch et al. created a technique based on fourfold texture analysis [9]. Wavelets (WL), local binary patterns (LBP), and the grey-level co-occurrence matrix are used to extract the bone characteristics. The histogram of gradients (HoG) and Haralick features (HAR). Then, a random forest (RF) classifier that combined 3D texture features with trabecular BMD data found a high probability of distinguishing those with low bone quality who are susceptible to vertebral fractures. The novel approach produced an AUC of 0.88, a sensitivity of 77%, and a specificity of 78% when tested on 154 individuals.

Regular CT images, specialized quantitative CT (QCT) scans, and Hounsfield Units from phantom research were used by Sollmann et al. to calculate bone mineral density (BMD) [10]. Convolutional Neural Networks (CNNs) were used in conjunction with picture processing and analysis for the first two datasets. In order to automate the segmentation and correction of contrast media as well as the labeling of vertebral bodies, they updated the CNN method. In order to calculate relative BMD for the third dataset, they employed a hardware-based technique in which they placed a hydroxyapatite block underneath the region under examination and measured the decrease in CT signal strength. When employed on routine CT scans, the CNN-based automated framework showed excellent accuracy in detecting vertebral fractures, especially those brought on by osteoporosis.

A novel melanoma segmentation algorithm was presented by Nawaz et al. using the ISIC 2017 and ISIC 2018 datasets [11]. On these datasets, their updated approach produced better segmentation accuracy. For the U-Net CNN, they chose DenseNet77 as the encoder, and the decoder divided the estimated key points that the encoder had found. A modified algorithm for feature extraction, segmentation, optimization, and classification was proposed by Siva Kumar and Rajesh Kumar. They used contrast enhancement and median filtering as preprocessing techniques. Their method produced better brain tumor segmentation and classification from MRI data, leading to increased accuracy with reduced processing time.

3. Methodology

Medical image processing begins with acquiring raw data from MRI or CT scans and converting it into a format suitable for analysis by specialized software. Applying filters to minimize and remove unnecessary noise or artifacts.

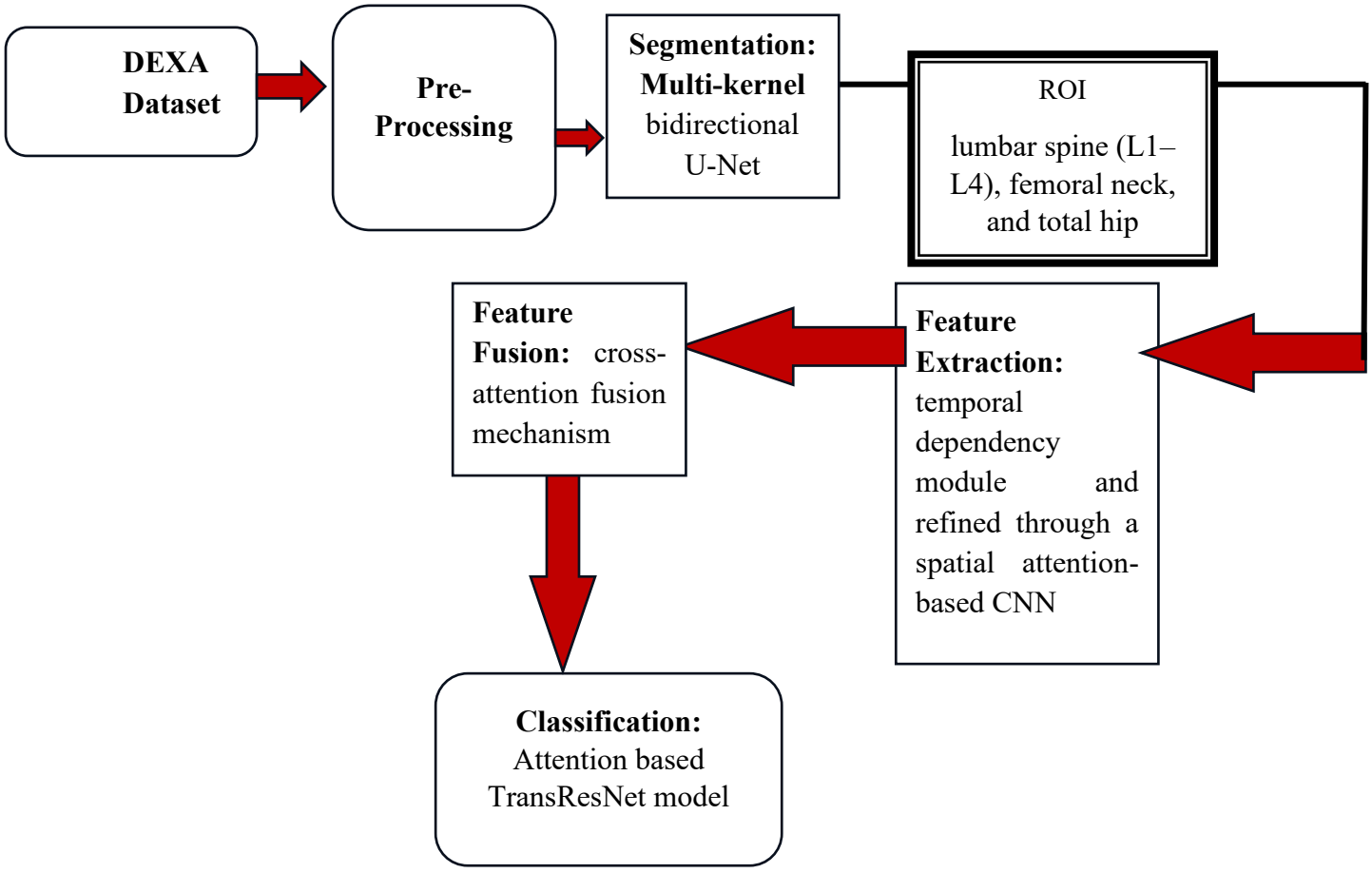

Figure 1: proposed flow

The processed images are often used for medical purposes to segment and annotate different anatomical areas, such as bones and tissues. Identifying and delineating various anatomical regions using segmentation techniques, including automated methods that leverage Artificial Intelligence and machine learning. These procedures improve the diagnostic and treatment planning accuracy and usefulness of medical imaging.

3.1. DEXA Dataset

Research on osteoporosis can benefit from this data. The Discovery of Hologic the DEXA photos were obtained using the Wi DXA bone densitometry system, which has 64 detectors and generates high-quality scans for accurate bone density readings. Notable applications that enhance patient evaluation and care by assessing vertebral fractures and abdominal aortic calcifications (AAC) are High-Definition Instant Vertebral Assessment, Advanced Body Composition Evaluation, and FRAX fracture risk assessment [21]. Ten seconds at 0.04 mGy is the standard exposure time for assessing the bone health of the femur and lumbar spine. The device requires 60°F to 90°F, 100 VAC (16A) electricity, 20–80% relative humidity, and an average heat load of 3,400 BTU/hr in order to operate. Figure 2 shows DEXA images from the dataset that are both normal and osteoporotic.

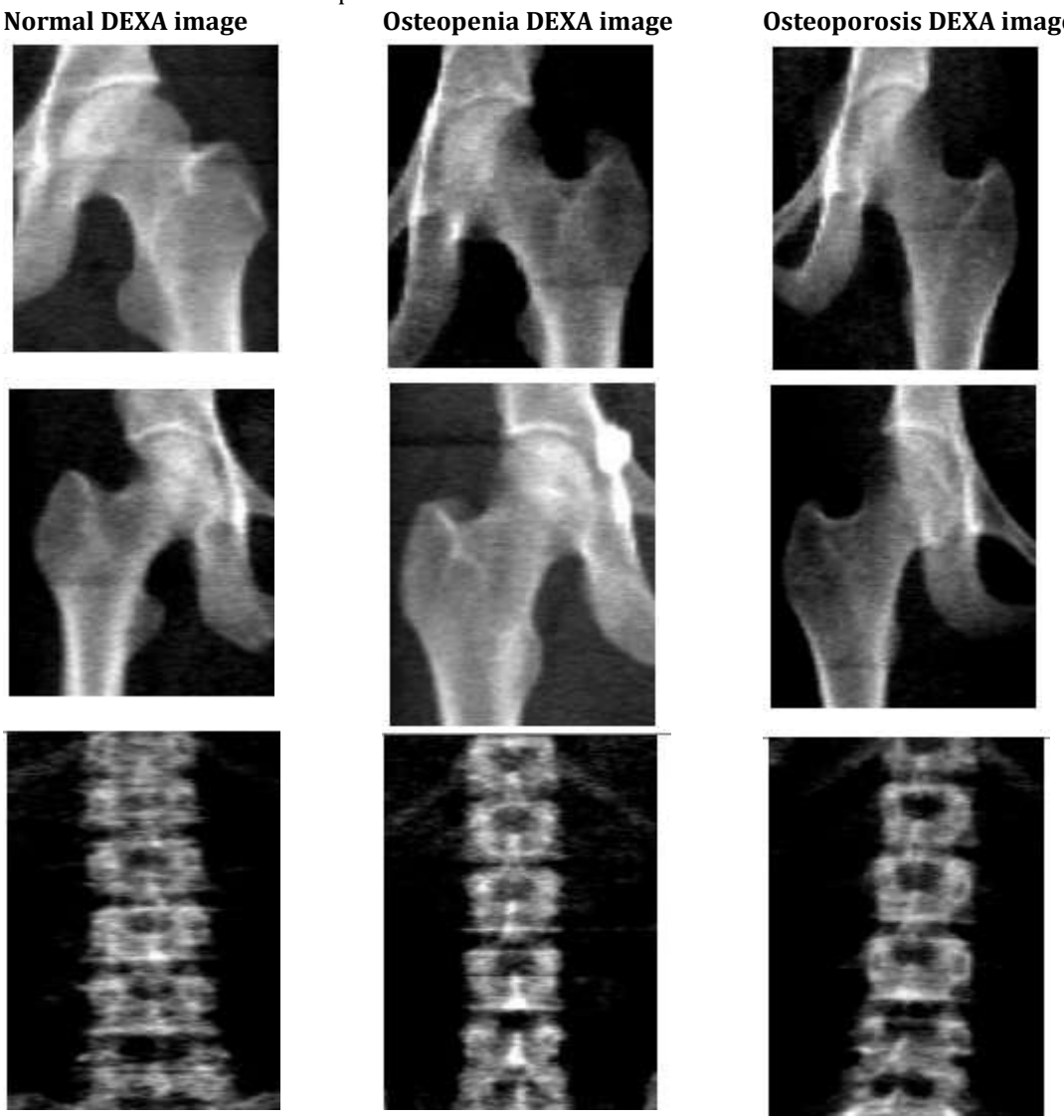

Figure 2: Normal and Osteoporotic clinical DEXA images

3.2. Adaptive Bilateral Filter based Preprocessing

A method for smoothing images while maintaining edges is called bilateral filtering. In order to avoid edge blurring, this filter computes a spatially weighted average that takes into account the geometric proximity and intensity similarity of nearby pixels. In contrast, conventional low-pass filtering $f(\delta)$, assumes that a pixel's intensity at a particular place is comparable to that of its nearby pixels, resulting in consistent smoothing throughout the image. Equation (1) expresses this assumption and the associated filtering action.

$$h(x) = k_d^{-1}(x)|| \int_{-\infty}^{\infty} f(\delta)c(\delta, x)d\delta \quad (1)$$

where $(c(\delta, x)$ calculates the mathematical relationship between a nearby point and the area center (x), and (k_d^{-1}) is a constant. The output picture (h) and the input image (f) could both be multiband. Additionally, Equation (2) expresses this link.

$$k_d(x) = || \int_{-\infty}^{\infty} c(\delta, x)d\delta \quad (2)$$

A popular method for improving edges in digital image processing is the adaptive unsharp masking concept. By subtracting a blurred (diffused) version of the image from the original, this method enhances image sharpness by highlighting edge features. Equation (3) represents the unsharp masking model's mathematical formulation.

$$len\ (x, y) = I(x, y) + \propto x\ (I(x, y) - Ism(x, Y)) \quad (3)$$

Here, $I(x, y)$, $Ism(x, y)\ and\ len(x, y)$ Take note of the improved, smoothed, and original images, respectively.

3.3. Segmentation: Multi kernel bidirectional U-Net

Medical picture segmentation has recently seen tremendous advancements because to deep learning. In this sense, the most well-known deep neural network architecture, U-Net, is most familiar to the medical imaging industry. Despite its overall success in segmenting multimodal medical pictures, experiments on challenging datasets showed that the conventional U-Net framework seems to be lacking in some areas. As a result, we suggest certain changes to the state-of-the-art U-Net model [23]. The technical approach improves accuracy and completeness in identifying and analyzing structures across many imaging modalities by accurately segmenting multimodal biomedical images using a Multi-Dimensional U-Convolutional Neural Network. Because of the advancements, we propose a new framework called Multi-Dimensional U-Convolutional Neural Network (MDU-CNN) as a potential successor for the U-Net framework. On a sizable collection of multimodal medical images, we contrasted the conventional U-Net with our proposed framework, MDU-CNN. When it comes to excellent photographs, there have been little adjustments, but when it comes to challenging images, there has been a significant improvement.

The final step of the decoder network is linked to a SoftMax layer that transforms the output into probability maps. The brain tumor model in this model is trained via cross entropy loss, which is described as:

$$L_{bce} = -\sum_{i=1}^{b}\sum_{j=1}^{n} GT_{ij}\ log\left(predi_{ij}\right) + \left(1 - GT_{ij}\right) log(1 - predi_{ij}) \quad (4)$$

Where GTɐ9 is ground truth pixel of ith batch of jth pixel of the image and prediɐ9 is predicted output pixel of ith batch of jth pixel of the image; n is the number of pixels in the photos, and b is the batch size. The outputs of the modified U-Net model are obtained by applying the sigmoid function to the weighted sums of the hidden layer activations,

$$predi_i = \frac{1}{1+e^{-\theta_i}} \quad (5)$$

$$\theta_i = \sum_{j=1} w_{ij}\ h_j \quad (6)$$

We may determine the derivative of the error for each weight that connects the hidden and output units using the chain rule.

$$\frac{\partial L_{bce}}{\partial w_{ij}} = \frac{\partial L_{bce}}{\partial predi_{ij}} \frac{\partial predi_{ij}}{\partial \theta_{ij}} \frac{\partial \theta_{ij}}{\partial w_{ij}} \quad (7)$$

When compared to the original U-Net architecture, the Improved U-Net has demonstrated increased accuracy. The network is now more efficient because fewer parameters and calculations are required thanks to the usage of depth-wise separable convolutions and residual connections [24]. The network's capacity to segment intricate structures has been enhanced by the attention mechanism.

Pseudo-inverses provide closed-form solutions for the subproblems P1 through P3. Simple least-square minimizations are involved in these subproblems. They can also be successfully solved by conjugate gradient methods. Rearranging sub-problem P4 also presents a least squares minimization assignment.

$$\|\left(X\sqrt{\lambda L}\sqrt{\mu}\ (\phi(W_{i-h}X) + B\ \right) - \left(W_{h-o}\sqrt{\lambda D}\ \sqrt{\mu I}\ \right)Z\|_F^2 \quad (8)$$

When compared to the original U-Net architecture, the Improved U-Net has demonstrated increased accuracy. The network is now more efficient because fewer parameters and calculations are required

thanks to the usage of depth-wise separable convolutions and residual connections [24]. The network's capacity to segment intricate structures has been enhanced by the attention mechanism.
Pseudo-inverses provide closed-form solutions for the subproblems P1 through P3. Simple least-square minimizations are involved in these subproblems. They can also be successfully solved by conjugate gradient methods. Rearranging sub-problem P4 also presents a least squares minimization assignment.

$$B \leftarrow Z - \emptyset(W_{i-h}X) - B \quad (9)$$

There are two established exit conditions: Iterations continue until the difference in the goal function falls below a predetermined threshold across U-Net iterations, or until they reach a predetermined maximum number.

3.4. Feature Extraction: temporal dependency module and refined through a spatial attention-based convolutional neural network

This stage is especially made to handle the enormous volume and intricacy of digital pathology data, including gigapixel whole-slide pictures, without sacrificing system stability or contextual information. The hybrid model offers a balanced and thorough representation of disease patterns by combining Transformer-based global attention for modeling long-range tissue architecture with convolutional neural networks (CNNs) for identifying fine-grained cellular and morphological information. In a clinical setting, this guarantees consistent performance across a range of patient demographics and slide characteristics. The two most often used techniques are average pool and maximum pool [25]. The three levels of the CNN model are the pool, activation, and convolution layers. Newly received data is integrated into the network via a number of filters. These filters are similar to conventional HR filters. They are discovered through independent investigation rather than being made public. The convolution layer uses feature detector maps with variable kernel sizes or visual input at various locations to capture local characteristics. The formula is as follows:

$$f_1^k(p,q) = \sum_c \sum_{x,y} i_c(x,y) \,.\, e_1^k(u,v) \quad (10)$$

$$F_1^k = [f_1^k(1,1), \ldots (f_1^k(p,q), .. f_1^k(P,Q))]. \quad (11)$$

$$N_l^k = \frac{F_l^k - \mu_B}{\sqrt{\sigma_B^2 + \varepsilon}} \quad (12)$$

In this instance, the index of the first layer's k convolution kernel is multiplied by each element of the input image tensor.
To do this, we first use the channel-wise attention method to highlight more informative channels on the CNN-based features. The squeeze and excitation technique is used to carry out the normalization process. First, we assess each channel's importance using the global contextual representation of each feature map:

$$g\,f = \frac{1}{H \times W} \sum_i^H \sum_j^W x\,f\,(i\,,j) \quad (13)$$

where H ×W represents the spatial dimension of the channel and g f represents the global contextual information.

$$s\,f\; = \sigma\,(W_2\,\delta\,(W_1\,g\,f\,)) \quad (14)$$

Here, W1 and W2 stand for the completely connected weights and δ and σ for the sigmoid and Relu activations, respectively. To determine coefficients, they employed the CNN feature map: Ψf = f s. The boundary distribution B∗ is multiplied by the output feature map of the Transformer module to enhance the boundary representation: f = Ψf.
Deep learning is one of the most recent methods for value prediction. Compared to other machine learning algorithms, Convolution Neural Networks, one of the deep learning methods used for sampling, yield superior results. Batch normalization for a transformed feature-map F_l^k is shown in equation (15).

$$N_l^k = \frac{F_l^k - \mu_B}{\sqrt{\sigma_B^2 + \varepsilon}} \quad (15)$$

CNN was first trained on screening data from the US and a different multi-center dataset from Europe. In order to improve early detection with trustworthy machine learning models and save lives, this study investigates early-stage lung cancer diagnosis using CNNs. Each variable's contribution can be used to express the chain rule:

$$\frac{\partial e}{\partial x_{i,j,k}^{\ell}} = \frac{\partial e}{\partial y_{i,j,k}^{\ell}} \frac{\partial f(y_{i,j,k}^{l})}{\partial y_{i,j,k}^{\ell}} = \frac{\partial e}{\partial y_{i,j,k}^{\ell}} f'(x_{i,j,k}^{l}) \quad (16)$$

Even while CNN models have demonstrated exceptional accuracy on controlled datasets, there is still a major barrier to their use in real-world scenarios involving a range of patient populations [26]. In order to mitigate this, validation across many datasets and methodologies is required to provide resilience against unexpected variations in imaging data:

The 3D input CNN x assumes to calculate the non-linear input $x_{i,j,k}^{\ell}$to $(i,k)\ th$ unit in the level ℓ, the following is added:

$x_{i,j,k}^{\ell} = \sum_a \sum_b \sum_c \omega_{a,b,c} y_{(i+a)(j+b)(k+c)}^{\ell-1} + b^{\ell}$ (17)

The result of the $(i,j)^{th}$unit in the ℓ^{th} This is how the convolutional layer appears:

$y_{i,j,k}^{\ell} = f(x_{i,j,k}^{\ell})$ (18)

Hereditary factors also play a major role in lung cancer. Unchecked tissue proliferation is the cause of lung cancer. Lung cancers can be either malignant or noncancerous:

$f_1^k(p,q,r) = \sum_c \sum_{x,y,z} i_c(x,y,z) \,.\, e_1^k(u,v,w)$ (19)

The expression for a convolutional operation is

$$F_1^k = [f_1^k(1,1,1), \dots (f_1^k(p,q,r), .. f_1^k(P,Q,R))] \quad (20)$$

This study created an automated method for using grayscale CT scan images to identify cancer.

$Z_l^k = g_p(F_l^k)$ (21)

The activation function for a convolved feature-map is defined by equation (22).

$T_l^k = g_a(F_l^k)$ (22)

The equation above F_l^k is an output of convolution that is allocated to the activation function g_a (.) that transforms the output and adds non-linearity T_l^k for lth layer.

3.5. Feature Fusion: cross-attention fusion mechanism

By enabling one source to selectively attend to the other, a cross-attention fusion process combines complimentary information from two distinct feature sources. The attention operation allows the model to highlight the most instructive and contextually significant aspects of the second modality by calculating relevance scores between the query and key features. After that, these weighted features are combined to create a fused representation that better captures correlations and inter-source relationships than straightforward concatenation or averaging. Therefore, in tasks like classification, detection, and multi-modal learning, cross-attention fusion increases feature alignment, decreases redundancy, and boosts overall model performance.

$$Q = XW_Q, \quad K = YW_K, \quad V = YW_V \quad (23)$$

$$Cross - Attention(X,Y) = softmax\left(\frac{QK^T}{\sqrt{d}}\right) V \quad (24)$$

$$Z = softmax\left(\frac{XW_Q\ (YW_K)^2}{\sqrt{d}}\right) \quad (25)$$

By enabling one feature set to selectively attend to the other, the cross-attention fusion method combines data from two distinct feature sources. Here, learnable weight matrices are used to project features Y into keys K and values V, while input features X are projected into queries Q.

$$Z = AV \quad (26)$$

This adaptive weighting captures long-range dependencies, maintains contextual links during fusion, and promotes semantic alignment across modalities.

$$Z_h = softmax\left(\frac{Q_h K_h^T}{\sqrt{d_h}}\right) V_h \quad (27)$$

$$Z = Concat\ (Z_1, \dots Z_H) W_o \quad (28)$$

$$Z' = LayerNorm(Z + X) \quad (29)$$

Because simple fusion strategies are unable to capture complex inter-feature relationships in complex tasks like multi-sensor remote sensing analysis, multimodal perception, and cross-domain representation learning, cross-attention is especially effective in producing a richer and more discriminative joint representation.

.

$$\alpha_h = softmax(S_h) \quad (30)$$

$$Z_{res} = Z + X \quad (31)$$

$$Z_{OUT} = LayerNorm\ (Z_{res}) \quad (32)$$

$$Z_{final} = FFN\ (Z_{OUT}) + Z_{OUT} \quad (33)$$

With multi-head attention, residual connections, normalization, and a feed-forward refinement stage, these equations depict an entire cross-attention fusion block.

3.4: Classification: attention based TransResNet model

Artificial intelligence approaches offer fascinating new potential for the identification of biological systems from raw data since they can detect significantly more complex patterns of association than conventional statistical tests can. Even though these networks have been used to analyse high-dimensional omics data,

it is still unknown how to assess these models' results in a biological context. Here, we provide a CNN-based feature selection technique for nonimage data. Our pipeline, Deep Feature, can generate sets of the most important genes that are used internally to make predictions in addition to successfully transforming omics data into a format that is perfect for training a CNN model [27]. To obtain better classification performance, TransResNet for enhanced classification combines the advantages of Residual Networks (ResNet) and Transformer-based architectures. By fusing TransResNet's deep feature extraction capabilities with Transformers' self-attention processes, this hybrid model surpasses conventional techniques in capturing both local details and global context. In jobs where long-range connections and hierarchical features are crucial, TransResNet is particularly good at managing complex datasets, learning sophisticated patterns, and enhancing generalization. Take the example of medical data input A, which has multiple properties and is expressed as

$$\int_{-\infty}^{t_h} p\left(\frac{x}{\omega_b}\right) = \alpha \qquad (34)$$

with t_h the threshold, ω_b the background class, x the pixel gray-level and α the significance. Equation (34) provides the error probability for the vessel class.

TransResNet, or residual networks, which are composed of residual blocks, have reduced the difficulty of training very deep networks. The first thing that stands out as being different is the direct connection, which forgoes a few layers in between (which may change depending on the model). The "skip connection," which forms the foundation for residual blocks, is this link.The output of the layer has been changed by this skip connection. If this skip link is not used, the input "x" is multiplied by the layer's weights before a bias term is added. The result of applying the activation function, f(.), to this term is H(x).

$$H(X) = F(WX + B) \text{ or} \qquad (35)$$

$$H(X) = F(X) \qquad (36)$$

Now with the introduction of skip connection, the output is changed to

$$H(X) = F(X) + X \qquad (37)$$

When the input and output dimensions diverge, as can occur with convolutional and pooling layers, there seems to be a small issue with the TransResNet approach. There are two options when the dimensions of f(x) differ from x.

$$H(X) = F(X) = W1.X \qquad (38)$$

In contrast to the first strategy, which does not include any additional parameters, in this instance we include one, w1. The learning of identity functions by layers has been found to be significantly aided by residual blocks. This is evident from the formulas above. In basic networks, the outcome is.

$$H(X) = F(X), \qquad (39)$$

Consequently, f(x) must equal x in order to train an identity function, which is more difficult than with TransResNet, which has output:

$$H(X) = F(X) + X, \qquad (40)$$

$$F(X) = 0 \qquad (41)$$

$$H(X) = X \qquad (42)$$

In the best scenario, a deep neural network with more layers can greatly reduce error and approach the mapping of "x" to output "y" more precisely than one with fewer levels. As a result, we expect TransResNet to outperform basic deep neural networks. When compared to traditional neural networks with simple layers, TransResNet greatly improves the performance of neural networks with additional layers, as seen by a notable decrease in error % [28]. TransResNet clearly has a much lower error % than plain-34 in networks with 34 layers. Furthermore, we can see that TransResNet and plain-18 have about comparable error percentages.

A feedforward, unsupervised neural network called an autoencoder is used to extract features from previously processed data. According to previous studies, adding more hidden layers significantly increases computation but has no effect on final performance. As a result, a three-layered autoencoder was implemented. Using an autoencoder improves the prediction performance of classification models.

$$H = f(WX + b) \qquad (43)$$

TransResNet clearly has a much lower error % than plain-34 in networks with 34 layers. Furthermore, we can see that TransResNet and plain-18 have about comparable error percentages.

A feedforward, unsupervised neural network called an autoencoder is used to extract features from previously processed data. According to previous studies, adding more hidden layers significantly increases computation but has no effect on final performance. As a result, a three-layered autoencoder was implemented. Using an autoencoder improves the prediction performance of classification models.

$$\hat{X} = g(W'H + b') \qquad (44)$$

In this context, $\hat{X}$ represents the acquired feature representation, while W', b', and g(·) refer to the decoder's weight, bias, and decoding function, accordingly. In order to reduce the reconstruction error, we establish a cost function through the process of
where N is the number of patients. It has been shown that the TransResNet value is dependable and may be utilized to explain the gastric cancer forecasts in a number of machine learning techniques. Despite this, the number of characteristics (K) in standard computations grows exponentially [29–32]. This method is easily included into widely used tools that make it easier to understand the risk factors for stomach cancer. The relationship between a feature x_i and TransResNet value in GLM $\emptyset_{GLM}$ is as follows:

$$\emptyset_{GLM}(x_i^{(j)}) = a_i x_i^{(j)} - E(a_i x_i) = a_i x_i^{(j)} a_i E(x_i) \quad (45)$$

The TransResNet value is consistently the feature influences the model's predictions.

$$X_i' = \frac{X_i - X_{min}}{X_{max} - X_{min}}, \quad F = W_1 X_1' + W_2 X_2' + \ldots + W_n X_n' \quad (46)$$

Data normalization balanced feature inputs for machine learning or deep learning models, especially in healthcare analytics and diagnostic pipelines.

$$Z_i = \frac{X_i - \mu_i}{\sigma_i}, \quad F = [Z_1 || Z_2 || \ldots || Z_n] \quad (47)$$

Deep learning models are made possible by this fusion technique, which maintains all of the information from each type of input. TransResNet is very useful for multimodal diagnosis, prognosis prediction, and decision-support systems because it can learn cross-modal correlations.

4. Result and discussion

Many scientists and engineers use Python to build models, create algorithms, and analyze data. Python is used to implement the suggested tasks, utilizing libraries like TensorFlow and Keras. The system configuration consists of Google Colab for deep learning model development, Ryzen 5/6 series CPU, NVIDIA GTX GPU, and Windows 10 or Linux operating system. Performance metrics analyzed include error rate, processing time, and error frequency, with model development parameters set to 10 epochs and a learning rate of 0.09. In figure 3 osteoporosis assessment include the lumbar spine (L1–L4), femoral neck, and total hip, as these regions are highly indicative of bone density changes due to estrogen deficiency.

Test Site	Input image	Preprocessed image	Segmented image	Remarks
Left Hip	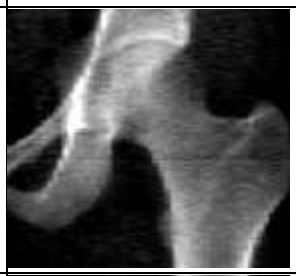	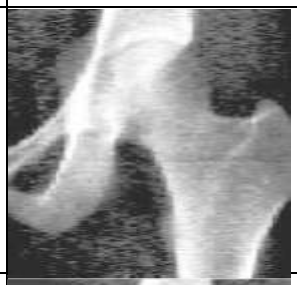	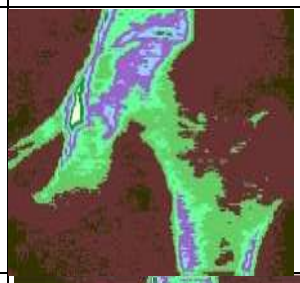	Osteoporosis
Right Hip	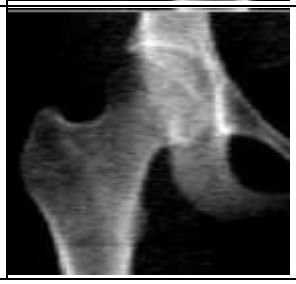	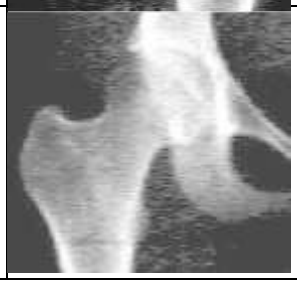	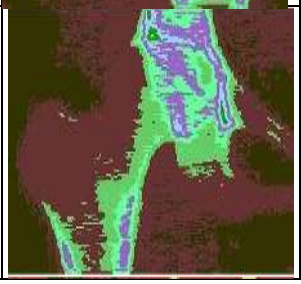	Osteoporosis

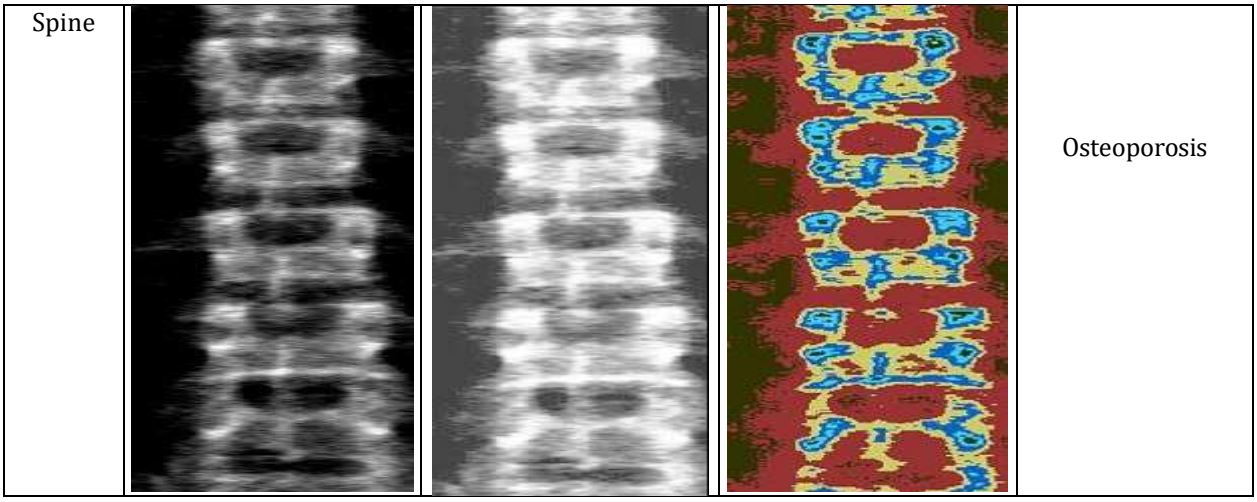

Figure 3: Segmented result

After being improved, the input images are fed into a bidirectional U-Net model. Accurately choosing and segmenting the ROI using bidirectional U-Net guarantees that the model concentrates on the most clinically important areas of the picture rather than unimportant portions. Figure 5 displays the outcomes of the recommended approach.

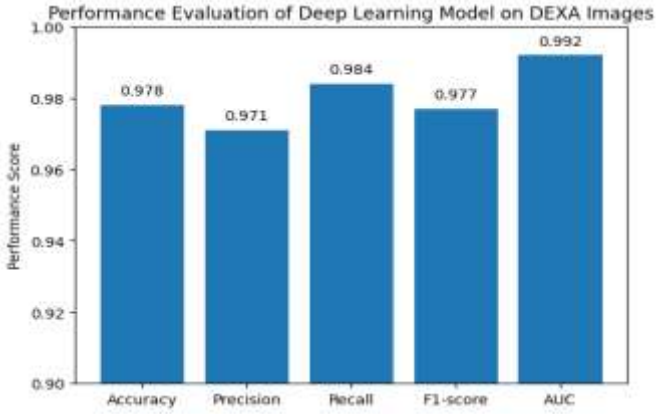

Figure 4: Performance Evaluation of Deep Learning Model on DEXA Images

Figure 4 represents a deep learning model has performed based on five standard evaluation metrics. From the chart, Accuracy is approximately 0.978, Precision is 0.971, Recall is 0.984, F1-score is 0.977, and AUC is the highest with a value of 0.992. Overall, the chart demonstrates that the proposed deep learning model is highly accurate, reliable, and efficient for analyzing DEXA images.

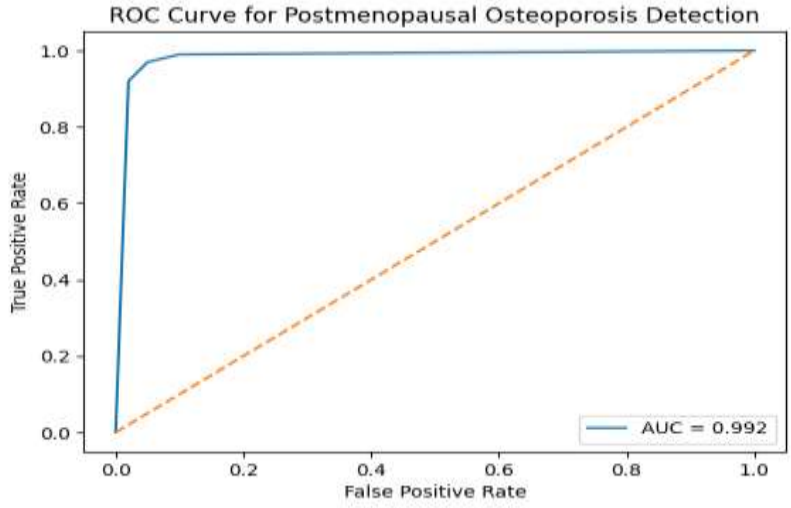

Figure 5: ROC Curve for Postmenopausal Osteoporosis Detection

The suggested attention-based TransResNet model outperformed other models in a number of evaluation criteria and showed remarkable efficacy. Our model obtained great performance and stability by utilizing DNN incorporating the advantages. The ROC curve for postmenopausal osteoporosis detection demonstrates a high sensitivity with a very low false positive rate. The AUC of 0.992 confirms the excellent diagnostic accuracy and it can reliably distinguish between osteoporotic and non-osteoporotic cases.

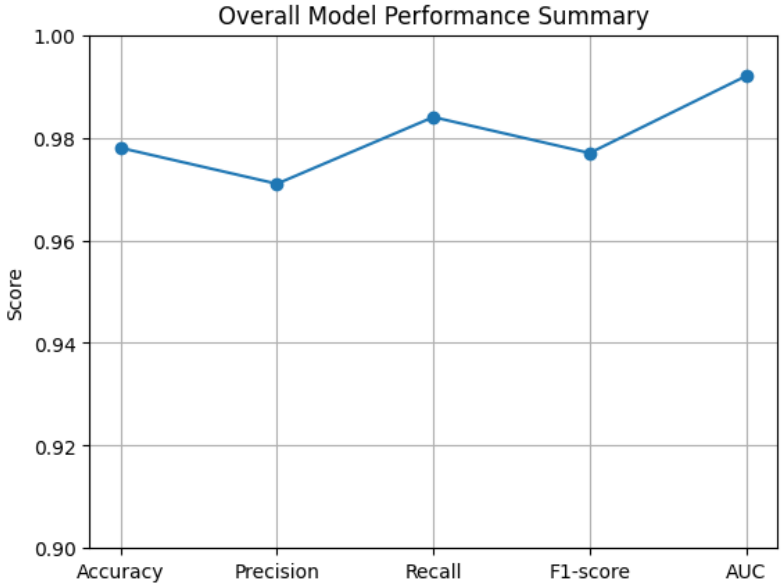

Figure 6: Overall, Model Performance

Figure 6 illustrates the performance of a deep learning model the line chart clearly demonstrates that the model performs consistently well across all evaluation parameters. Proving that it is reliable, accurate, and suitable for analyzing the given dataset.

Figure 7: Underfitting Scenario

The underfitting is shown in the figure 7 indicates low training and validation accuracies across epochs. Although both accuracies increase gradually with training suggesting limited learning capacity rather than overfitting. This behavior typically highlighting the need for a more complex model, improved feature representation, or extended training.

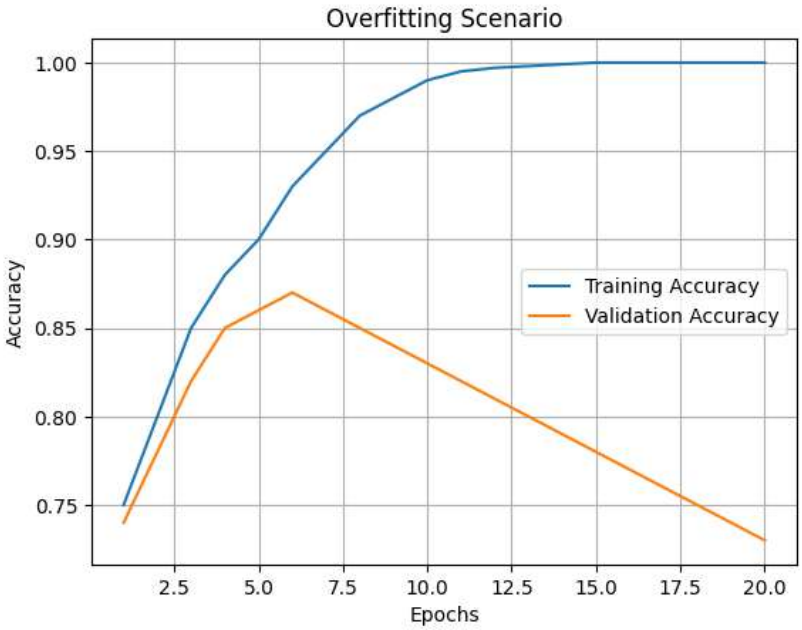

Figure 8: Overfitting Scenario

The loss over epochs graph shows how successfully the model learned and converged during training, with the 5% metric declining until the fifth epoch and then remaining low and stable. This small loss suggests that the model was highly successful in reducing loss, producing the expected results.

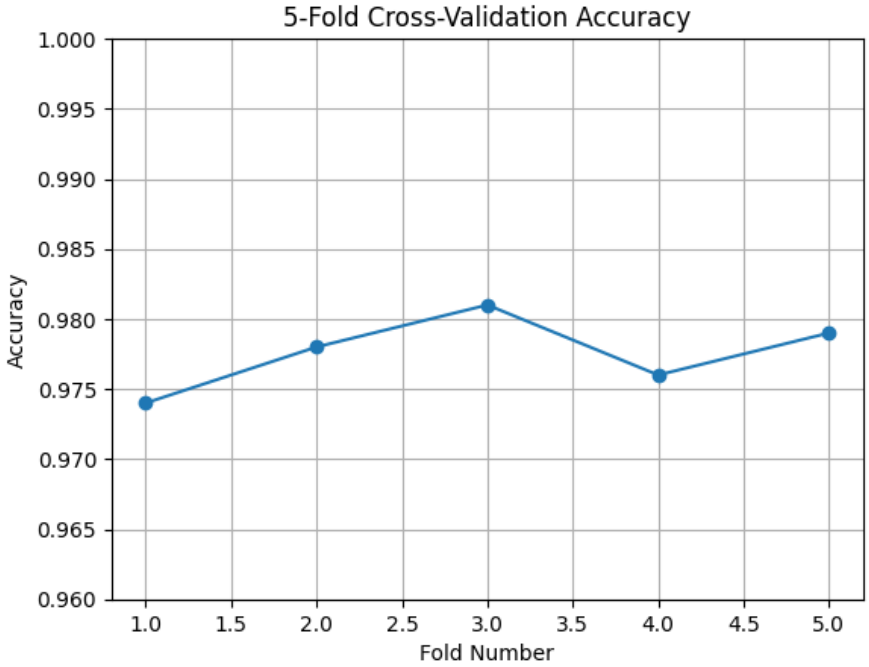

Figure 9: Fold Cross-Validation Accuracy

Improved osteoporosis detection and classification are made possible by the model's ability to detect minute variations in bone density and structure through analysis and comparison of these feature values across anatomical sites. When used on region-specific or combined datasets, this method makes use of the spatial attention-based convolutional neural network capacity to combine spatial and temporal cues, improving diagnostic accuracy.

Table 1: spatial attention-based convolutional neural network

Feature ID	Feature Name	Left Hip (Mean ± SD)	Right Hip (Mean ± SD)	Spine (Mean ± SD)
F1	Mean Pixel Intensity	126.32 ± 4.12	127.10 ± 4.05	129.45 ± 3.85
F2	Bone Edge Sharpness	0.842 ± 0.021	0.846 ± 0.019	0.854 ± 0.018
F3	Trabecular Texture Entropy	4.215 ± 0.082	4.208 ± 0.079	4.236 ± 0.075
F4	Cortical Thickness Variance	0.058 ± 0.005 mm^2	0.056 ± 0.004 mm^2	0.060 ± 0.004 mm^2
F5	Temporal Feature Decay	0.013 ± 0.002	0.012 ± 0.002	0.011 ± 0.001
F6	Fractal Dimension	1.742 ± 0.011	1.746 ± 0.010	1.752 ± 0.009
F7	Energy (Wavelet Band)	0.654 ± 0.013	0.650 ± 0.014	0.658 ± 0.012
F8	Haralick Contrast	0.119 ± 0.006	0.118 ± 0.006	0.120 ± 0.005
F9	Haralick Homogeneity	0.935 ± 0.004	0.936 ± 0.004	0.938 ± 0.003
F10	Temporal CNN Activation Avg	0.852 ± 0.009	0.854 ± 0.009	0.856 ± 0.008

Figure 10: Training and Validation Accuracy

The training and validation accuracy curves show a well-generalized model with effective learning behavior across epochs. Both accuracies increase steadily and remain closely aligned, indicating that the model is learning meaningful patterns without significant overfitting. There is just a slight difference between the validation and training accuracy, indicating high generalization to new data. When the curves progressively plateau at high accuracy levels, it means that the model has hit its peak performance and that additional training will not significantly enhance it. Overall, the plot reflects a stable and robust training process with high predictive accuracy.

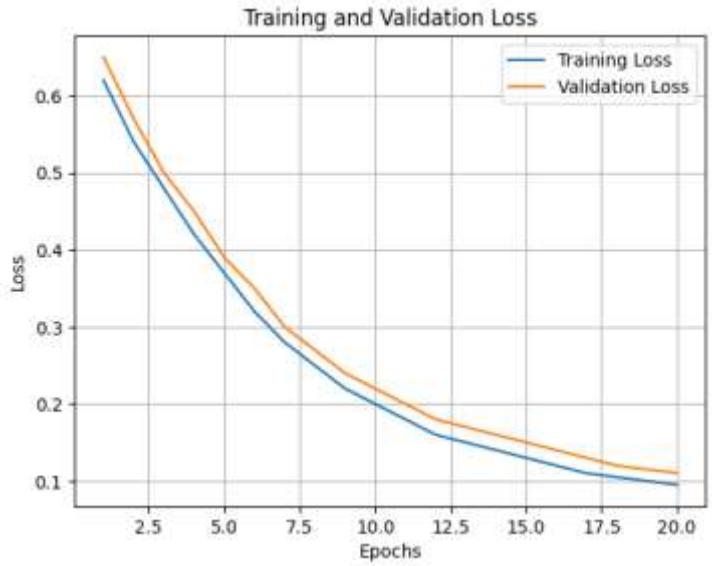

Figure 11: Training and Validation Loss

By detecting BMD using dual-energy X-ray absorption and successfully differentiating bone tissue from soft tissue, DXA scans provide precise classification of bone health. In contrast, radiographs use single-energy X-rays and are less effective for classifying bone mass, as they primarily provide anatomical imaging rather than precise BMD measurements. This study proposes an Attention with TransResNet framework for classifying BMD levels—normal, osteopenia, and osteoporosis—from DEXA images to support early detection of low bone mass.

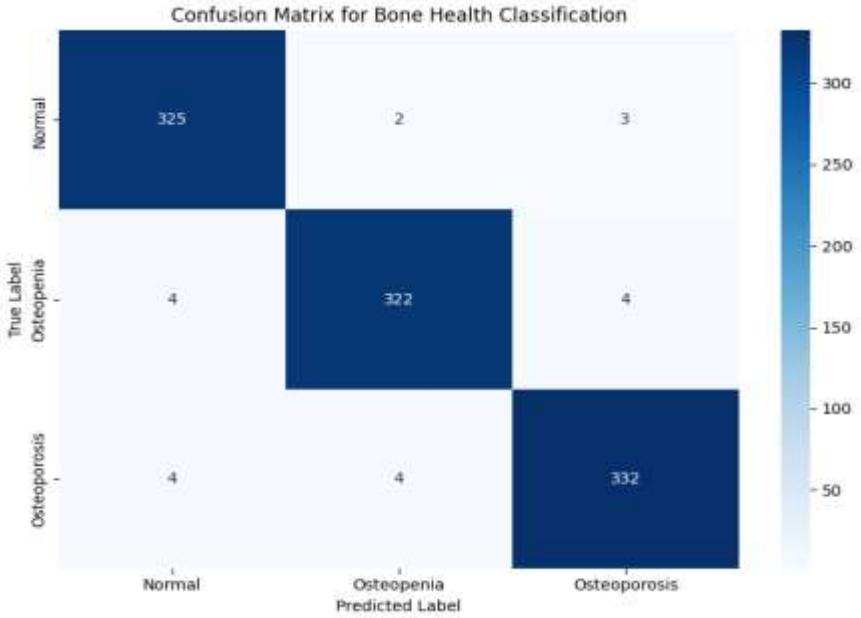

Figure 12: Confusion matrix

The model was very successful at differentiating Osteopenia from both Normal and Osteoporosis instances, a task that is clinically difficult because of minute variations in bone texture and density, according to an analysis of the confusion matrix in Figure 9. While the Attention with TransResNet component enhanced the representation of long-range dependencies within the image features, the CNN's attention mechanisms enabled the model to concentrate on important portions of the bone structure, such as the trabecular and cortical areas. These findings imply that the suggested model is both accurate and comprehensible, making it a potentially useful tool for early intervention planning and automated osteoporosis screening in clinical settings.

Table 2: Performance of proposed models

Class	Accuracy (%)	Precision (%)	Recall (%)	Specificity (%)	F1 Score (%)	Sensitivity (%)
Normal	99.12	98.85	98.65	99.35	98.75	97.82
Osteopenia	98.78	97.95	97.82	98.26	97.88	97.68
Osteoporosis	98.54	97.66	97.68	97.69	97.67	98.65
Overall	**98.96**	**98.15**	**98.05**	**98.43**	**98.90**	**98.05**

Table 2's findings support the model's potential application in clinical decision-making for osteoporosis screening and diagnosis by confirming its robustness and efficacy in differentiating between different amounts of bone mass. This likely explains the potential use of radiography for opportunistic osteoporosis and osteopenia screening. Sometimes, osteopenia or osteoporosis can be predicted using quantitative ultrasonography of the calcaneus. Incorporating deep learning for identifying osteoporosis in images not only enhances diagnostic accuracy with 98.96% and efficiency but also supports better patient outcomes through timely interventions. These representations will probably become increasingly important in healthcare as technological and scientific developments.

Table 3: comparison of accuracy and loss with state of art models

Models	Modality	Accuracy (%)
CNN [28]	X-ray	89.2
LSTM [29]	DEXA	81.98
DNN [30]	X-ray	82
DBN [31]	DEXA	83.6
Bi-LSTM [32]	DEXA	85.3
Proposed	**DEXA**	**98.96**

A comparative analysis of different deep learning models for bone health classification reveals significant performance variation across modalities. Models using X-ray images, such as CNN and DNN, achieved accuracies of 89.2% and 82%, respectively, demonstrating moderate effectiveness. On the other hand, models utilizing DEXA scans generally performed better for this task, with LSTM, DBN, and Bi-LSTM models achieving 81.98%, 83.6%, and 85.3% accuracy, respectively. Notably, the proposed model, which uses a Attention with TransResNet architecture on DEXA images, significantly outperforms all others with an accuracy of 98.96%, highlighting the value of both the imaging modality and the advanced attention-based framework for accurate bone mass classification.

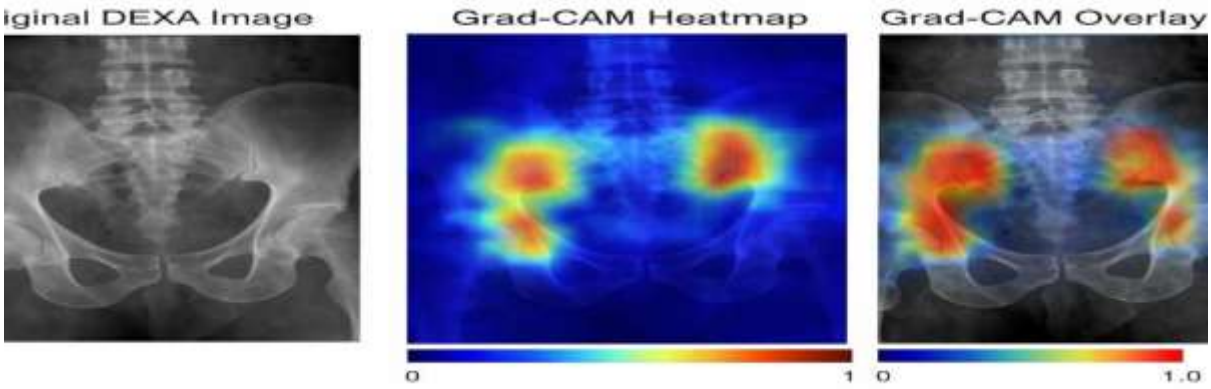

Figure 13: Iginal DEXA Image, Grad-CAM Heatmap, Grad-CAM Overlay

By automatically extracting pertinent features from DEXA images, algorithms that use deep learning eliminate the necessity for human feature development. They are able to spot minute variations in bone structure and density that human experts might miss. Clinical choices can be made more quickly thanks to automated analysis, which can drastically cut down on the time needed for diagnosis.

5. Conclusion

This work offers an innovative deep learning architecture that greatly improves the diagnosis and evaluation of postmenopausal osteoporosis from DEXA scans. By combining multi-task learning with bone segmentation, fracture point localization, and osteoporosis level prediction, the proposed architecture overcomes the drawbacks of traditional BMD-based diagnostic approaches. The addition of bidirectional U-Net bone segmentation, self-supervised pretraining, spatial attention mechanisms, and cross-attention fusion of clinical and image modalities allows for better detection of the subtle structural pattern's indicative of bone fragility. The excellent performance results obtained by the proposed architecture clearly establish its validity and efficacy for practical clinical use. Expert validation further verifies its applicability in practical settings. In conclusion, the suggested approach opens the door to improved patient care, customized treatment plans, and more effective computer-aided diagnostic systems for the management of osteoporosis by offering a dependable, comprehensible, and significant tool for early osteoporosis diagnosis and fracture risk assessment.

References

1. Yen, Tzu-Yun, Chan-Shien Ho, Yueh-Peng Chen, and Yu-Cheng Pei. "Diagnostic accuracy of deep learning for the prediction of osteoporosis using plain X-rays: a systematic review and meta-analysis." Diagnostics 14, no. 2 (2024): 207.
2. Amani, Firouz, Masoud Amanzadeh, Mahnaz Hamedan, and Paniz Amani. "Diagnostic accuracy of deep learning in prediction of osteoporosis: a systematic review and meta-analysis." BMC Musculoskeletal Disorders 25, no. 1 (2024): 991.
3. Belali, Md Habibullah, Ferdus Rhaman Khan, Nur Mohammed Rajin, Hridoy Sarkar, and Khandaker Mohammad Mohi Uddin. "Bone Osteoporosis Fractures Detection with Deep Learning: An X-ray Image Analysis Approach." Biomedical Materials & Devices (2025): 1-19.
4. Keerthika, S., A. Janani, Lalitha Krishnasamy, S. DevaBrindha, S. Priyanka, and S. R. Dharun. "Leveraging Advanced Deep Learning Architectures for Precise Knee Osteoporosis Prediction: A Paradigm Shift in Diagnostic Healthcare." In 2024 2nd International Conference on Advances in Computation, Communication and Information Technology (ICAICCIT), vol. 1, pp. 377-382. IEEE, 2024.
5. Shim, Jae-Geum, Dong Woo Kim, Kyoung-Ho Ryu, Eun-Ah Cho, Jin-Hee Ahn, Jeong-In Kim, and Sung Hyun Lee. "Application of machine learning approaches for osteoporosis risk prediction in postmenopausal women." Archives of osteoporosis 15, no. 1 (2020): 169.
6. Ogbonna, Chidiebere, and Ernest E. Onuiri. "Predictive Diagnostic Model for Early Osteoporosis Detection Using Deep Learning and Multimodal Imaging Data: A Systematic Review and Meta-Analysis." Asian Journal of Engineering and Applied Technology 13, no. 2 (2024): 28-35. Nazia Fathima, S. M., R. Tamilselvi, and M. Parisa Beham. "A Survey on Osteoporosis Detection Methods with a Focus on X-ray and DEXA Images." IETE Journal of Research 68, no. 6 (2022): 4640-4664.
7. Ullah, Kainat A., Faisal Rehman, Muhammad Anwar, Muhammad Faheem, and Naveed Riaz. "Machine learning-based prediction of osteoporosis in postmenopausal women with clinical examined features: a quantitative clinical study." Health Science Reports 6, no. 10 (2023): e1656.
8. Feng, Shang-Wen, Szu-Yin Lin, Yi-Hung Chiang, Meng-Han Lu, and Yu-Hsiang Chao. "Deep learning-based hip x-ray image analysis for predicting osteoporosis." Applied Sciences 14, no. 1 (2023): 133.
9. Ho, Chan-Shien, Tzuo-Yau Fan, Chang-Fu Kuo, Tzu-Yun Yen, Szu-Yi Chang, Yu-Cheng Pei, and Yueh-Peng Chen. "HarDNet-based deep learning model for osteoporosis screening and bone mineral density inference from hand radiographs." Bone 190 (2025): 117317.
10. Zhang, Yuji, Ming Ma, Xingchun Huang, Jinmin Liu, Cong Tian, Zhenkun Duan, Hongyin Fu, Lei Huang, and Bin Geng. "Machine learning is changing osteoporosis detection: an integrative review." Osteoporosis International (2025): 1-14.
11. Alden, Zahraa Noor Aldeen M. Shams, and Oguz Ata. "A comprehensive analysis and performance evaluation for osteoporosis prediction models." PeerJ Computer Science 10 (2024): e2338.
12. Villamor, E., Carlos Monserrat, L. Del Río, J. A. Romero-Martín, and María José Rupérez. "Prediction of osteoporotic hip fracture in postmenopausal women through patient-specific FE analyses and machine learning." Computer Methods and Programs in Biomedicine 193 (2020): 105484.

13. Pedoia, Valentina, Francesco Caliva, Galateia Kazakia, Andrew J. Burghardt, and Sharmila Majumdar. "Augmenting osteoporosis imaging with machine learning." Current osteoporosis reports 19, no. 6 (2021): 699-709.
14. Hong, Namki, Sang Wouk Cho, Sungjae Shin, Seunghyun Lee, Seol A. Jang, Seunghyun Roh, Young Han Lee et al. "Deep-learning-based detection of vertebral fracture and osteoporosis using lateral spine X-ray radiography." Journal of Bone and Mineral Research 38, no. 6 (2020): 887-895.
15. Liu, Lili. "Implemented classification techniques for osteoporosis using deep learning from the perspective of healthcare analytics." Technology and Health Care 32, no. 3 (2024): 1947-1965.
16. Varalakshmi, P., Smruthi Sathyamoorthy, V. Darshan, V. Ramanujan, and Sakthi Jaya Sundar Rajasekar. "Detection of osteoporosis with DEXA scan images using deep learning models." In 2022 International Conference on Advances in Computing, Communication and Applied Informatics (ACCAI), pp. 1-6. IEEE, 2022.
17. Theetchenya, S., J. Senthilkumar, V. Mohanraj, and Y. Suresh. "An In-Depth Examination of Diagnostic Methods and Therapeutic Approaches for Osteoporosis Utilizing Clinical Factors and Medical Imaging." In International Health Informatics Conference, pp. 273-283. Singapore: Springer Nature Singapore, 2023.
18. Erjiang, E., Tingyan Wang, Lan Yang, Mary Dempsey, Attracta Brennan, Ming Yu, Wing P. Chan et al. "Machine learning can improve clinical detection of low BMD: the DXA-HIP study." Journal of Clinical Densitometry 24, no. 4 (2021): 527-537.
19. Mohankumar, M. "A Systematic Review on Osteoporosis Prediction in Postmenopausal Women." In 2024 1st International Conference on Trends in Engineering Systems and Technologies (ICTEST), pp. 1-6. IEEE, 2024.
20. Ramachandran, Darsana, and J. Charles. "Advancements in Osteoporosis Prediction: Trends, Challenges and Future Perspectives." In 2025 International Conference on Machine Learning and Autonomous Systems (ICMLAS), pp. 686-692. IEEE, 2025.
21. Idoko, David Oche, Moyosoore Mopelola Adegbaju, Abdulrahman Abdullateef, Grace Chinenye Okafor, and I. Nduka. "Technological Innovations in Osteoporosis Diagnosis and their Implications for Bone Metastases Management in Oncology." International Journal of Innovative Science and Research Technology ISSN 2456-2165 (2024).
22. Areeckal, Anu Shaju, and Michel Kocher. "Current and emerging diagnostic imaging-based techniques for assessment of osteoporosis and fracture risk." IEEE reviews in biomedical engineering 12 (2018): 254-268.
23. Carvalho, Filipe Ricardo, and Paulo Jorge Gavaia. "Enhancing osteoporosis risk prediction using machine learning: A holistic approach integrating biomarkers and clinical data." Computers in Biology and Medicine 192 (2025): 110289.
24. Javed, Mazhar. "Osteoporosis prediction for trabecular bone using machine learning: a review." Computers, Materials & Continua (2021).
25. Alborzi, Melina, and Parsa Abadi. "OSTEO-AI: A Systematic Review and Meta-Analysis of Artificial Intelligence Models for Osteoarthritis and Osteoporosis Detection and Prognosis." Undergraduate Research in Natural and Clinical Science and Technology Journal 9 (2025): 1-14.
26. Umamaheswari, R., D. Lakshmi, V. Samuthira Pandi, B. Geetha, S. Sumithra, and Ragini PY. "An advanced deep learning approach for primary osteoporosis prediction using radiographs with clinical covariates." In 2023 7th International Conference on Electronics, Communication and Aerospace Technology (ICECA), pp. 788-793. IEEE, 2023.
27. Fang, Kaibin, Xiaoling Zheng, Xiaocong Lin, and Zhangsheng Dai. "A comprehensive approach for osteoporosis detection through chest CT analysis and bone turnover markers: harnessing radiomics and deep learning techniques." Frontiers in Endocrinology 15 (2024): 1296047.
28. Saranya, S., S. Christy, and V. Sheeja Kumari. "Deep Learning and Feature Extraction Techniques for Early Prediction of Osteoporosis from Medical Imaging." In 2025 International Conference on Intelligent Computing and Control Systems (ICICCS), pp. 1141-1146. IEEE, 2025.
29. Tarighatnia, Ali, Masoud Amanzadeh, Mahnaz Hamedan, Alireza Mohammadnia, and Nader D. Nader. "Deep learning-based evaluation of panoramic radiographs for osteoporosis screening: a systematic review and meta-analysis." BMC medical imaging 25, no. 1 (2025): 1-11.
30. He, Yu, Jiaxi Lin, Shiqi Zhu, Jinzhou Zhu, and Zhonghua Xu. "Deep learning in the radiologic diagnosis of osteoporosis: a literature review." Journal of International Medical Research 52, no. 4 (2024): 03000605241244754.
31. Jang, Ryoungwoo, Jae Ho Choi, Namkug Kim, Jae Suk Chang, Pil Whan Yoon, and Chul-Ho Kim. "Prediction of osteoporosis from simple hip radiography using deep learning algorithm." Scientific reports 11, no. 1 (2021): 19997.

32. Zhang, Bin, Keyan Yu, Zhenyuan Ning, Ke Wang, Yuhao Dong, Xian Liu, Shuxue Liu et al. "Deep learning of lumbar spine X-ray for osteopenia and osteoporosis screening: A multicenter retrospective cohort study." Bone 140 (2020): 115561.

Funding Declaration
This research did not receive any funding.

Declarations
Clinical trial number : Not applicable
Consent to Publish: Not applicable.
Consent to Participate: Not applicable.
Ethics Declaration : Not applicable.

Ethics Statement:
This study used the Mendeley data-Osteoporosis DEXA dataset , and No human participants were directly involved in this study, therefore, Ethics Approval and Consent to Participate are stated as “Not Applicable” in the manuscript.

Informed Consent:
This study used an existing Mendeley data-Osteoporosis DEXA dataset ; informed consent was handled by the original data source, and no direct participant recruitment was conducted by the authors.

Consent to Publish:
No identifiable images or participant information are included in the manuscript. Therefore, Consent to Publish is also mentioned as “Not Applicable” in the manuscript.

Data Availability Statement:
The datasets generated during and/or analysed during the current study are available in the Osteoporosis DEXA dataset repository

We will ensure that the same Data Availability Statement is provided both in the manuscript and in the submission system as instructed.